PIV AND WALL CONVECTIVE HEAT TRANSFER MEASUREMENTS IN A ROUND JET IN CROSS-FLOW

G.M. Carlomagno, F.G. Nese, T. Astarita
DETEC, University of Naples, p.le Tecchio 80-80125, Naples, Italy

Keywords: *PIV, infrared thermography, jets in cross-flow, convective heat transfer*

Abstract

In the present work the thermo-fluid-dynamic characteristics of the discharge of a round jet in a cross flow are studied. Particle Image Velocimetry (PIV) is used to evaluate the instantaneous velocity field and flow statistics, while convective heat transfer measurements are performed by means of infrared thermography. The main vortical structures and flow statistics are analysed for a Reynolds number, based on the pipe exit diameter and the cross stream velocity, which ranges from 1000 to 8000 and for injection ratio in the range 0.5-5. The convective heat transfer measurements over the wall the jet issues from are reported as Nusselt number maps normalised by the same dimensionless number measured without jet injection. The effect of the vortical structures on the wall convective heat transfer distribution is analysed and discussed.

1 Introduction

It is well known that many components of jet engines, rockets and space vehicles are exposed to high temperature. In order to improve technical and economical parameters of the turbine units and engine, an increase of the gas temperature in the combustion chamber and in the early turbine stages is required. As a consequence, the mechanical parts, such as turbine blades and combustion chamber walls, must be cooled. One of the most practical cooling method is effusion cooling, also named film cooling, where the cooling fluid is injected into the wall boundary layer through discrete holes or slots.

Previous investigations on film cooling mainly focused on temperature and velocity measurements in the near and far field of jets in crossflow. Many of the earliest studies were concerned with the determination of the adiabatic wall temperature, given in a dimensionless form as a film cooling effectiveness. The adiabatic wall temperature can be also used to infer the heat transfer coefficient. Eckert [1] was the first to give methods to predict heat transfer in film-cooled systems from adiabatic and isoenergetic heat transfer coefficients.

Since jets in cross-flow are also of great relevance for a lot of engineering applications (lifting jets in V/STOL aircraft, waste disposals, jets in combustors, etc.), many studies widely analysed the flow field and turbulence statistics in the vicinity of the jet exit. Many difficulties in the study of this complex phenomenon are due to the numerous parameters which influence the jet behaviour, the most important ones being the effective injection ratio, which is given by the jet to free stream velocity ratio in case of equal-density flows $R=v_j/u_\infty$, and the Reynolds number which is generally based on free stream velocity and hole diameter.

The investigation conducted by Goldstein and Taylor [2] was one of the first attempts to experimentally measure heat transfer coefficients in the neighbourhood of jets entering a cross flow. They found that jets increase the heat transfer coefficient in the region immediately adjacent to the holes and also at some distance downstream of the centreline of the holes. Leontiev [3] presented a review of calculation methods and experimental results for heat transfer under film cooling. The

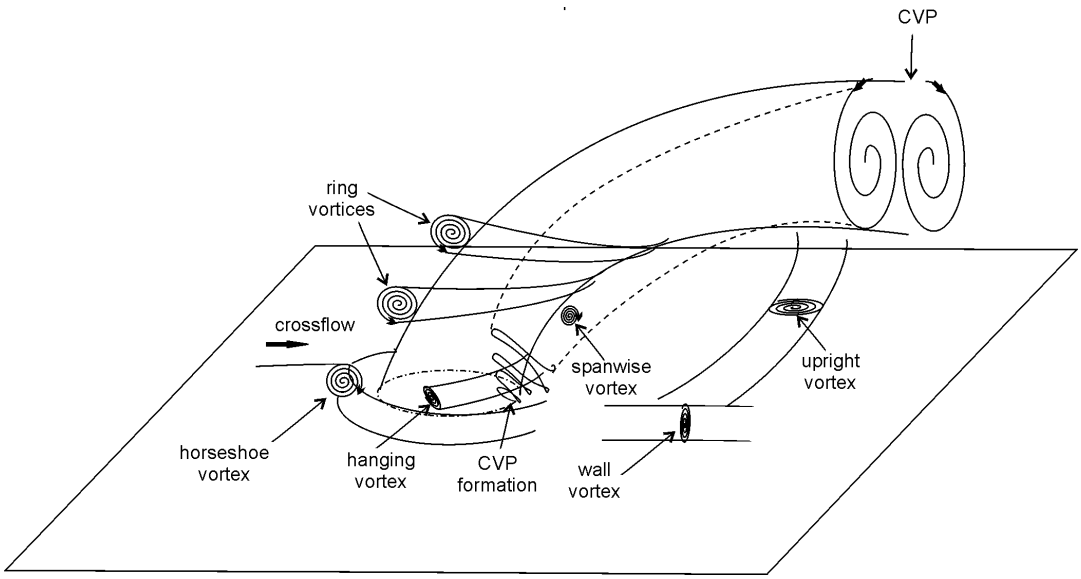

Fig.1. Schematic view of the main vortical structures originating from the interaction of the jet with the crossflow.

author proposed a generalised correlation for film cooling effectiveness which takes into account the influence of many parameters such as arrangement of film cooling, longitudinal pressure gradient, compressibility of the gas, surface roughness, etc. A parametric study of temperature distribution on effusion-cooled plates using infrared thermography was also performed by Gustaffson and Johansson [4] More recently, Astarita *et al.* [5] presented heat transfer maps for a jet normally issuing from the wall for *Re* about 5000 and *R* values ranging from 0.5 to 5.

In order to better understand the heat transfer problem, it is important to analyse both the flow field statistics and the vortical structures in proximity of the wall. This was widely performed both in experimental and numerical studies. Most of the earliest experimental investigations, [6-9], used flow visualization techniques or hot wire anemometry to study the mean flow patterns as well as to detect the vortical structures originating around the jet and the wall shear layers. The main vortical structures are sketched in Fig. 1. A 'horseshoe vortex' is envisaged near the wall, on the upstream side of the jet and on its lateral edges. A 'counter-rotating vortex pair' (CVP), which is bound to the lee surface of the jet, arises from a reorientation of the vorticity issuing from the pipe and from the vorticity generated at the interface between the cross-flow and the jet. 'Ring-like vortices' typical of free jets are observed around the jet external edges, while, in the wake region, 'wall vortices' and 'upright vortices' are detected. Numerical studies were conducted by Sykes *et al.* [10], Coelho and Hunt [11], Yuan and Street [12] and Yuan *et al.* [13]. The last authors found some new coherent vortical structures in the near field of the jet such as a pair of quasi-steady 'hanging vortices', which form in the skewed mixing layer between the jet and the crossflow nearby of the jet lateral edges, 'spanwise rollers' on the upstream and downstream edges of the jet as well as 'vertical streaks' in the main jet body.

Previous studies mainly focused on heat transfer in film cooling problems with multiple jets or on the fluid mechanics of a single jet such as flow field and turbulence statistics measurements. The present study differs from the preceding ones in that it is aimed at finding connections between turbulence statistics and convective heat transfer in the near field of a round jet perpendicularly issuing into a cross-flow. The study also analyses the effect of the injection ratio and of the Reynolds number on the thermo-fluid-dynamics of the jet in the vicinity of the wall, as well as it shows the effect of the vortical structures on the wall convective heat transfer distribution.

2 Experimental set-up

Experiments are carried out in the aspirated subsonic open circuit wind tunnel, with a rectangular test section of 300x400mm^2, of the 'Dipartimento di Energetica, Termofluidodinamica Applicata e Condizionamenti Ambientali' of the University of Naples Federico II. The tunnel inlet nozzle has a contraction ratio of 10 and a low turbulence intensity level (0.1%). The jet issues from a cylindrical pipe, having a diameter D=24mm, placed on the centreline of the 300mm side and 240mm downstream of the nozzle throat. Upstream of the jet exit hole, the wall boundary layer is laminar and its thickness is 8.6mm at Re=8000. The jet air, supplied by a compressor, goes sequentially through a pressure-regulating valve, a heat exchanger, a flow-meter, a plenum chamber, where the temperature is measured, and then through the pipe into the wind tunnel section. The heat exchanger allows the jet air to have the same temperature of the free stream, so as to realize an equal-density flow. Experimental tests are performed at Reynolds number going from 1000 to 8000. In order to reach such values the free-stream velocity is set to values from 0.6 to 5m/s while the mean jet exit velocity ranges from 0.3 to 25m/s, so to obtain injection ratios ranging from 0.5 to 5. The free-stream velocity is computed by means of pressure measurements metered with a transducer. The jet flow rate is metered by means of a rotameter.

2.1 PIV measurements

The schematic view of the PIV layouts with the adopted coordinate system and the positions of the laser arm and of the camera are shown in Fig. 2. The flow statistics used for comparisons with heat transfer measurements are measured in the plane normal to the jet at y/D=0.25 (see Fig. 2a), which constitutes the closest achievable measurement distance from the wall. For each value of the injection ratio and Reynolds number, the ensemble of realizations for the turbulent statistics and mean flow field consists of 500 images which are recorded with an acquisition rate of 2Hz. Turbulence and trajectory characteristics of the jet have also

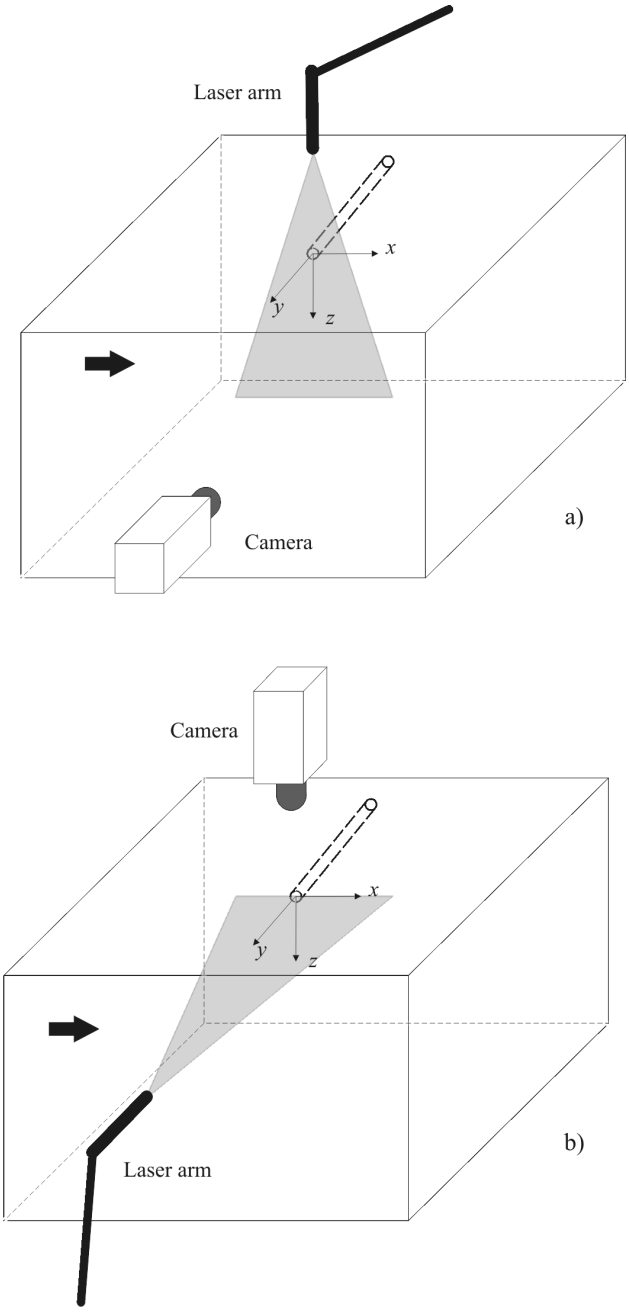

Fig.2. Schematic view of the PIV layout. a) measurements in the planes normal to the jet axis; b) measurements in the symmetry plane.

been studied in the symmetry plane z/D=0 (see Fig. 2b) with the same type of acquisition. The number of vectors computed from a couple of images is 80 × 60, while the distance between two adjacent vectors is in the range of 0.4 to 1.8mm (i.e., from 60 to 13 vectors per D respectively), depending on the image magnification factor.

Seeding made up of oil droplets, about 1μm in diameter, is injected into both the main

flow and the jet flow. The light sheet, which is generated by a neodymium:yttrium-aluminum-garnet (Nd-YAG) laser, has a thickness of about 1.5*mm*, a pulse duration of 6*ns*, a wave length of 532*nm* and a maximum energy per pulse of about 200*mJ*. PIV images are recorded with a CCD PCO-Sensicam camera using an *f*-number of 2.8. The CCD sensor consists of 1280 × 1024 pixels having a physical dimension of 6.7 × 6.7μm. Each image is digitised at 12 bits, so that a rather high number of grey levels (4096) may be used. The acquired images are interrogated by a high accuracy PIV algorithm. This method first calculates the cross-correlation of two homologous windows, in which each image is subdivided. Once the cross-correlation map is obtained, a peak detection operation, using a fractional displacement estimator, is performed over the map to determine the precise location of the maximum. The result of the correlation is used to build a displacement predictor over all the image pixels through a bilinear interpolation, so as to perform a translation, a rotation and a deformation of the interrogation windows. An iterative algorithm, including windows size reduction, allows to achieve high resolution measurements. In the present experiments, the starting square interrogation area has a linear dimension of 64 pixels, while the final one of 16 pixels. Furthermore, an outliers detection is applied after each intermediate step of the iteration process. Spurious vectors detected by means of a statistical validation criterion are replaced with a bilinear interpolation of valid neighbouring vectors. In the present data set the number of spurious vectors ranges from 5 to 10% depending on the velocity ratio, and the laser parameters. The maximum error in the velocity evaluation is found to be less than ±4%.

2.2 Infrared thermography

Convective heat transfer coefficient measurements are carried out by means of infrared thermography applied to the steady heated thin foil technique. Heat transfer measurements are performed over the wall the jet issues from. In order to allow for this study,

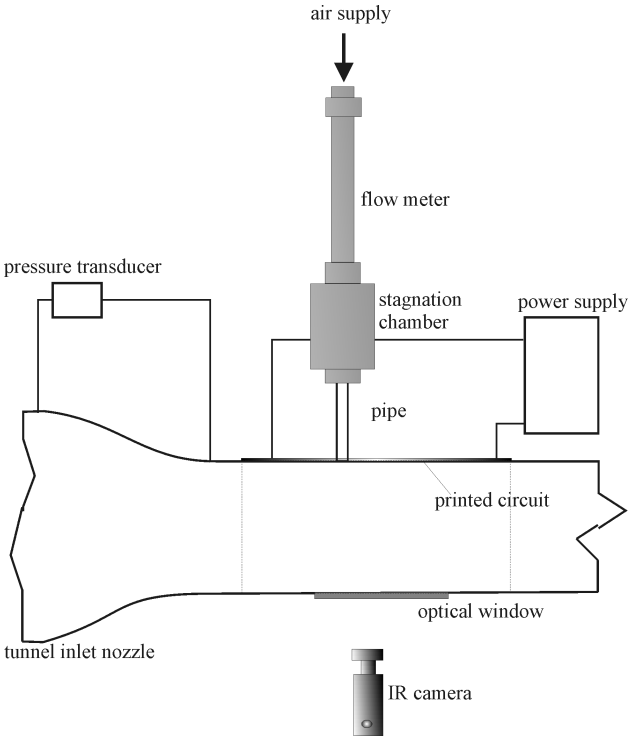

Fig.3. Sketch of the test section.

one side wall of the tunnel is made up of a printed circuit board insulated at its back and with a hole for the jet injection. The printed circuit board (300x600mm^2) is placed immediately downstream of the tunnel throat and is designed so as to achieve a constant heat flux over its surface. The copper tracks that constitute the circuit are 5μm thick, 1.8*mm* wide and located 2*mm* from each other. The board has an overall thickness of 0.5*mm* and is thermally insulated at its back. The electric current to the circuit is supplied by a stabilized DC power source and the dissipated power is computed by measuring voltage drop and amperage. The surface viewed by the infrared camera is coated with a thin layer of opaque paint, which has a total emissivity coefficient ε=0.95 in the wavelength of interest. The test section optical access window for infrared measurements is made up of bioriented polyetilene and a preliminary calibration of the radiometer takes into account also its presence. The experimental apparatus, together with the IR camera, is sketched in Fig.3. During the tests, particular care is taken to keep the plenum jet temperature equal to the free stream one within ±0.1°C.

The infrared thermographic system used for image acquisition is the Agema Thermovision 900LW. Images are scanned with a mercury-cadmium-telluride (Hg-Cd-Te) detector in the 8-12μm window. Each image is recorded as a 136 × 272 pixels per frame at 12 bits (4096 levels) and is time-averaged over 32 frames and low-pass filtered so as to reduce noise.

The thermal sensor adopted for convective heat transfer measurements is the heated thin foil. The convective heat transfer coefficient h between the foil and the free stream can be calculated from the recorded temperature maps by means of the following equation:

$$h = \frac{\dot{q} - \dot{q}_l}{T_w - T_{aw}} \qquad (1)$$

where $\dot{q}$ is the joule heating flux; $\dot{q}_l$ are the heat losses; T_w and T_{aw} are the wall and the adiabatic wall temperatures respectively. The quantity $\dot{q}_l$ includes radiative losses $\dot{q}_r$ and tangential conduction losses $\dot{q}_c$. Losses due to natural convection were found to be negligible for the tested Reynolds numbers.

The thermal radiative losses $\dot{q}_r$ may be evaluated as:

$$\dot{q}_r = \varepsilon\sigma\left(T_w^4 - T_a^4\right) \qquad (2)$$

where σ is the Stefan-Boltzman constant and ε is the emissivity coefficient. The tangential conduction within the board $\dot{q}_c$ is given by:

$$\dot{q}_c = -\left(\lambda_p \frac{\partial^2 T_w}{\partial x^2} + \lambda_n \frac{\partial^2 T_w}{\partial y^2}\right) \qquad (3)$$

where λ_p and λ_n are the bulk thermal conductance coefficients along the tracks and along the direction normal to them respectively (see Astarita and Cardone, [14]).

Convective heat transfer coefficients are put in the dimensionless form by means of the local Nusselt number defined as:

$$Nu = \frac{hD}{k} \qquad (4)$$

where k is the air thermal conductivity evaluated at film temperature (i.e. the mean temperature between the wall and the adiabatic wall temperature) and D is the pipe diameter.

Heat transfer results will be presented in terms of a normalized Nusselt number Nu/Nu_o where Nu_o is the Nusselt number without injection which is measured in the absence of the injection pipe as well. The maximum error in the Nu evaluation is found to be less than ±5%.

3 Results

3.1 Flow field measurements

In this section PIV measurements are reported for the tested injection ratios and Reynolds numbers. In all the figures which refer to

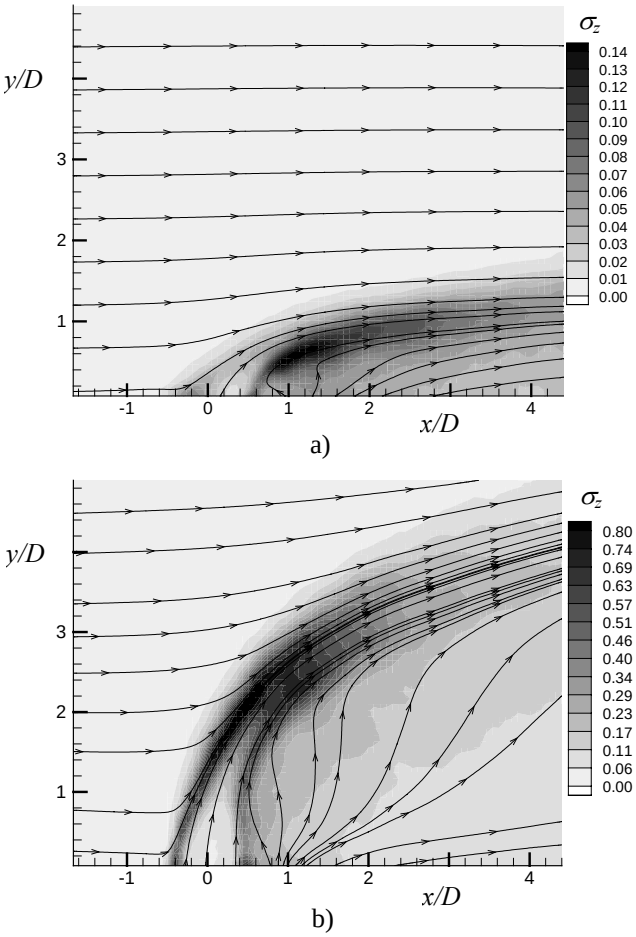

Fig.4. Mean in-plane streamlines and in-plane turbulent kinetic energy at the centreplane z/D=0 for Re=8000. a) R=1; b) R=3.

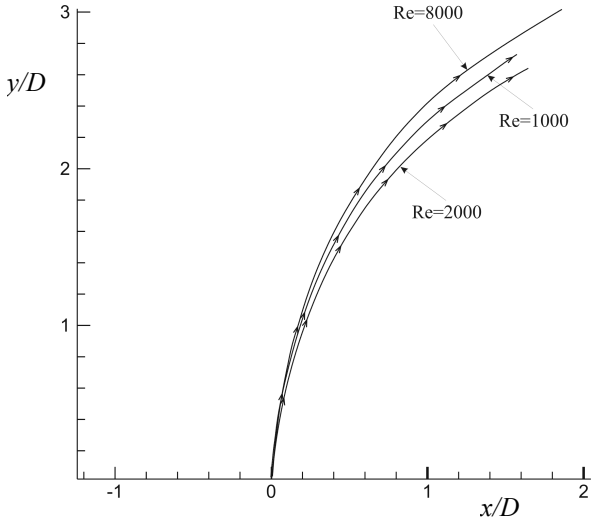

Fig.5. Streamline jet trajectories originating from the jet exit centre at various Reynolds numbers for R=3.

measurements on the planes with y/D=constant, the dashed and dotted circle indicates the pipe exit position. The cartesian coordinate system is the one shown in Fig. 2 and the spatial coordinates are non-dimensionalised by the pipe exit diameter D. The quantities σ_y and σ_z, which represent the turbulent kinetic energy in the planes y/D=const and z/D=0 respectively, and the turbulent shear stresses are made dimensionless by the square of the cross-flow velocity. The symbol $\overline{\ }$ denotes an ensemble average. The envelopes of the velocity vectors in the measurement planes, which in the following will be referred to as streamline patterns, are also shown.

In order to explain the wall temperature distribution which will be shown in the next section, it is useful to briefly recall the behaviour of the jet in the symmetry plane for increasing velocity ratios. As shown in Fig. 4, where the in-plane mean streamlines and turbulent kinetic energy are reported for Re=8000, for increasing R the jet penetrates further into the cross-stream; as a consequence a wide low pressure region originates in the back of the jet which causes a reverse flow, while a high turbulence region can be found mostly in the shear layer between the jet and the cross flow rather than in the wake. At lower Reynolds numbers the turbulent kinetic energy maps in the symmetry plane are qualitatively similar, while the bending over of the jet changes very

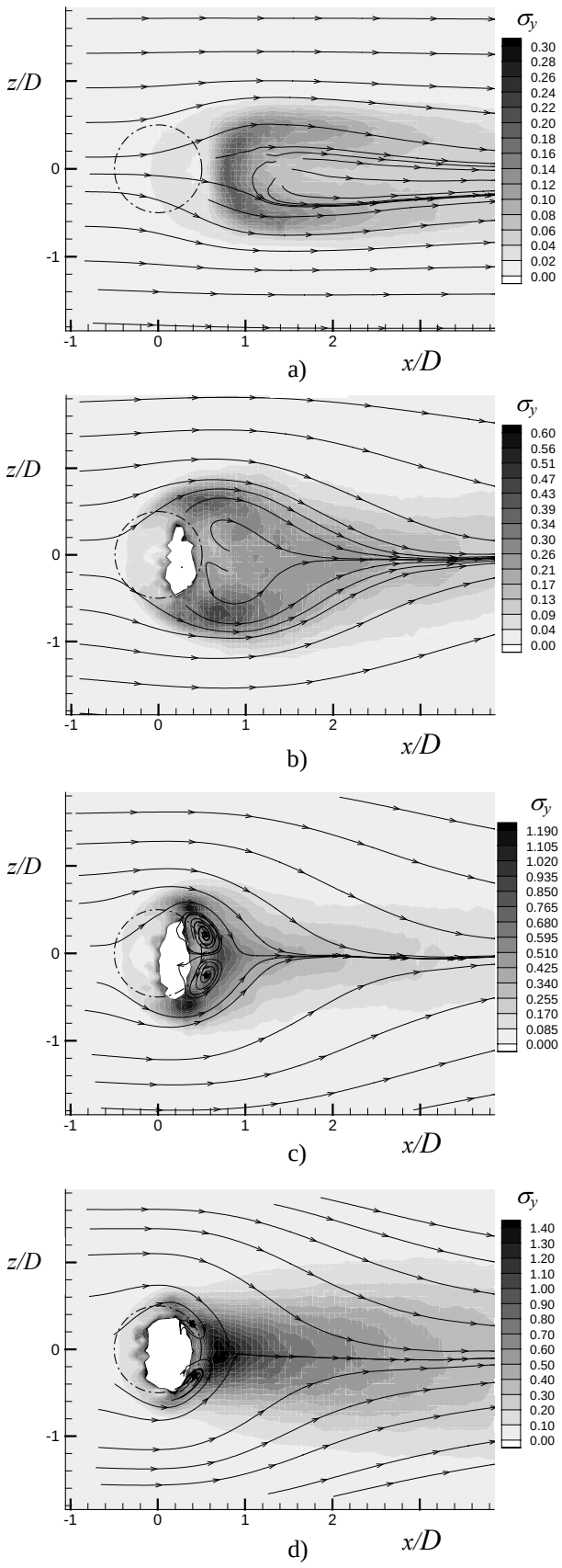

Fig.6. In-plane turbulent kinetic energy σ_y for Re=8000 at the plane y/D=0.25: a) R=1; b) R=2; c) R=3; d) R=4.

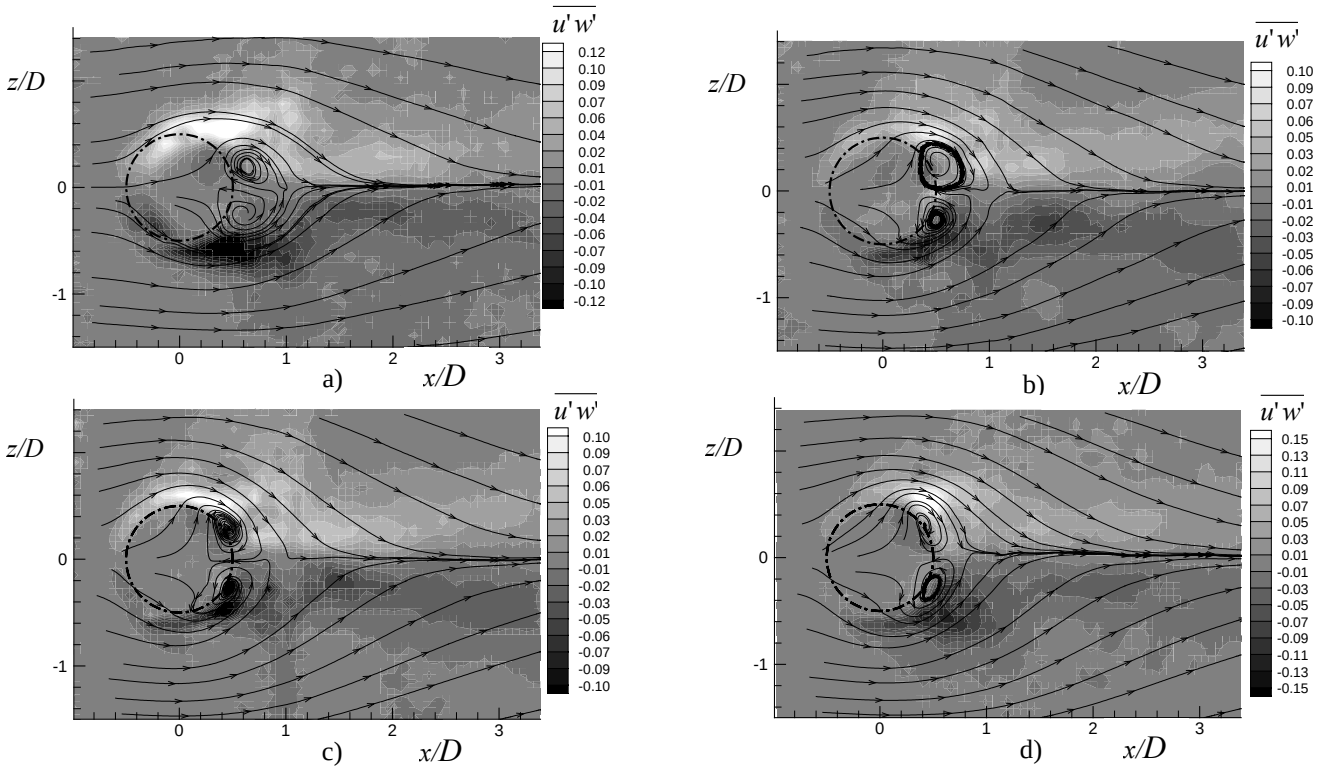

Fig.7. CVP evolution and shear stresses at the plane y/D=0.25 for R=3: a) Re=1000; b) Re=2000; c) Re=4000; d) Re=8000. The dashed and dotted line denotes the pipe exit section location.

slightly as shown in Fig. 5 for R=3.

The turbulent kinetic energy maps at the plane y/D=0.25 are plotted in Fig. 6 for R going from 1 to 4; the map at R=5 is not reported being similar to the one at R=4. As it is shown, two side maxima can be found for R=1 and R=2 (see Fig. 6a and Fig. 6b). These maxima, which are respectively reached at about 0.9 and 0.7 diameters downstream of the pipe axis, are shifted downstream with respect to pipe exit section, because for R=1 and R=2 the jet has a very strong curvature (e. g. see Fig. 4a) and the σ_y measurement plane is located 6mm far from the tunnel wall. For R>3 a maximum of the turbulent kinetic energy is present at about x/D=1 and its highest level is reached for R=4.

In Fig.7 the CVP evolution is analysed for R=3 and increasing Reynolds numbers in proximity of the wall (y/D=0.25). For Re=2000 the counter rotating vortices have a circular shape and are about of the same size as the pipe diameter. For higher Reynolds numbers the CVP evolves into an elliptic shape increasing its dimension along the z direction; as a consequence the jet obstruction increases and both the wake region and the jet influence region grow in size. The different characteristic of the CVP is connected to its formation mechanisms: at higher Reynolds number the CVP generation is most probably delayed and is not completely evolved into a circular vortical structure.

3.2 Heat transfer measurements

In this section heat transfer maps are reported, but results are not shown in the map white areas because there is either no heating there, or they are affected by edge effects (due to the strong tangential conduction).

The influence of R is analysed in Fig. 8 for Reynolds number set to 8000 and an injection ratio R ranging from 0.5 to 4; no significant differences are found between R=4 and R=5, hence only R=4 is reported. Two high heat transfer zones, which start from the lateral edges of the pipe and extend downstream of it, are present for R=0.5 and R=1. These zones tend to disappear for increasing injection ratio.

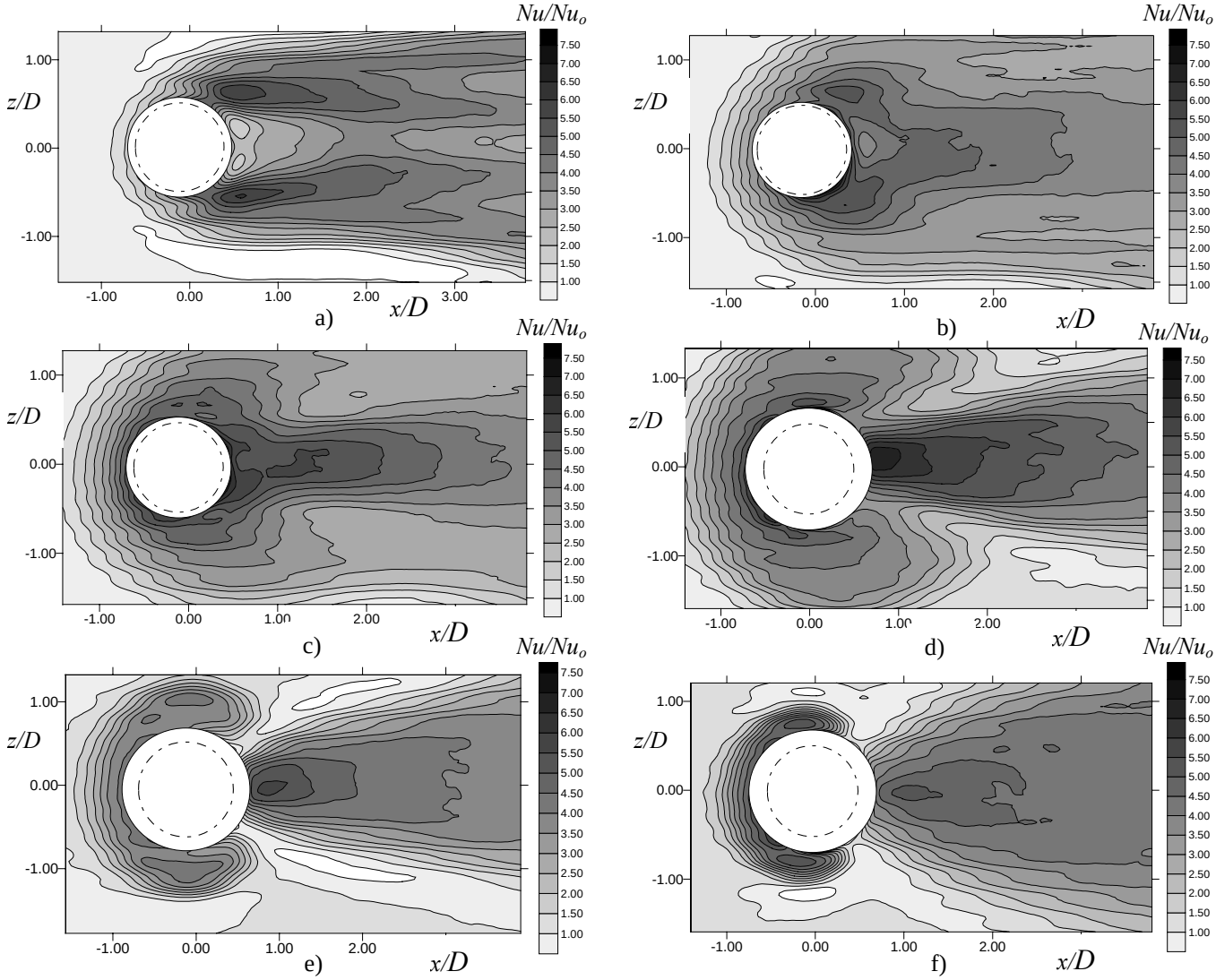

Fig.8. Normalised Nusselt number maps Nu/Nu_o over the heated plate for Re=8000: a) R=0.5; b) R=1; c) R=1.5; d) R=2; e) R=3; f) R=4.

Downstream of the pipe, on the centreline at about x/D=1, a low heat transfer region is found for R=0.5 which reduces for R=1. For increasing injection ratio, at about the same location, the minimum becomes a maximum (by reaching its highest value for R=2) that weakens and moves slightly downstream. The overall heat transfer at the wall appears to reduce going from R=1 to 3 and then increase from 3 to 5. This latter increase is most probably due to the upward motion in the jet wake, which becomes stronger for increasing injection ratio. On the jet upstream side, the convective heat transfer over the wall decreases for $R>2$, since the rising obstruction of the jet at high velocity ratios reduces the crossflow velocity more significantly.

The aforementioned heat transfer characteristics can be better understood by analysing both the flow field at the symmetry plane and the CVP behaviour at different velocity ratios. The presence of the two side high heat transfer zones which are found for R=1 can be connected with the corresponding turbulent kinetic energy map where two side maxima are found in the mixing region. In contrast to the high injection ratio cases, for R=1, downstream of the pipe exit, the jet is quite close to the tunnel wall and it induces high widespread turbulence levels in the vicinity of the wall. The local minimum value is probably due to a stagnation region beneath the jet

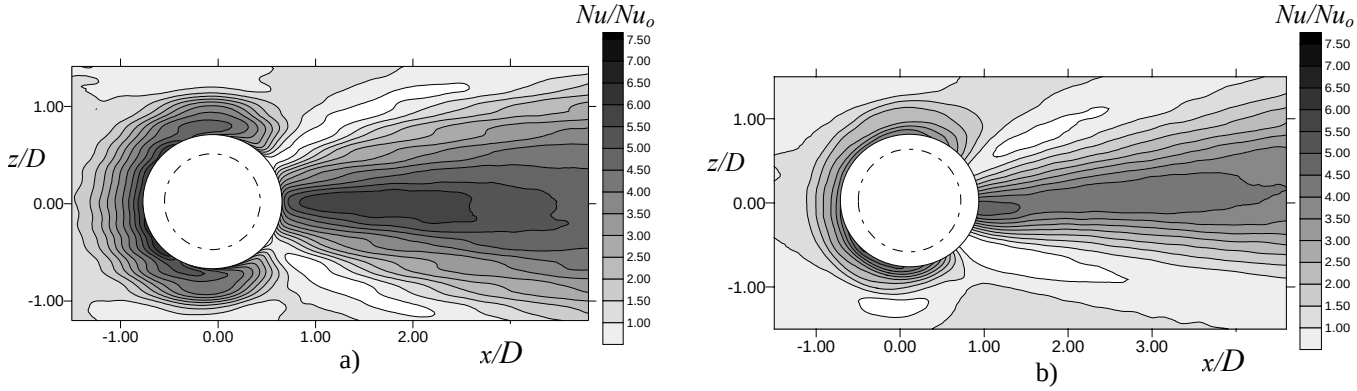

Fig.9. Normalised Nusselt number maps Nu/Nu_o over the heated plate for R=3: a) Re=4000; b) R=2000.

downward side at about x/D=1. In this case there is no evidence of the CVP formation, hence in that region no additional contribution to turbulence and heat transfer can be found. For R=2 on the jet lee side the highest values are reached among all the other injection ratios because the CVP and the node which is located at x/D=1 contribute to enhance the turbulence level. In addition, the low pressure region is not very high and cooling is mostly due to the jet flow, which has not been heated by the wall, rather than to the cross flow which enters the wake region.

It is believed that CVP formation is the reason why for higher injection ratios the heat transfer peak weakens or even disappears. In fact, as it is shown in Fig. 6c-d, for high ratios the CVP formation is delayed, it moves upstream and it is very close to the jet leeward side, as a consequence its contribution to heat turbulence is lower and the high Nusselt number region moves downstream. In addition, the strong upward motion in the back region of the jet has also a more stabilizing effect on the flow. The turbulent kinetic energy level maps do not explain the high heat transfer region upstream of the jet exit; this discrepancy may be attributed to the position of the measurement plane which is not fully inside the boundary layer, but in the vicinity of its edge, and this shows a strong influence mainly in the upstream region because, at the downstream side, the jet injection makes the boundary layer to break down.

For the highest tested injection ratio, i.e. R=5, on both the sides of the pipe at about z/D=±1, the heat transfer weakens practically recovering the values pertinent to no jet injection. A similar behaviour is found for R=4 while, for injection ratio equal to 3, this low heat transfer region is delayed downstream. This might be ascribed to a kind of free stream separation that is induced by the high momentum of the issuing jet and to the velocity distribution which has a primary role in the heat transfer outside the wake region.

The minimum found downstream of the pipe exit covers the largest area at R=0.5 because of a widespread stagnation region originating immediately downstream of the injection. At this injection ratio, close to the lateral edges of the jet thermal wake, two low heat transfer regions, which extend downstream for three diameters, can be detected. These regions are not visualized at higher injection ratios. Furthermore, at R=1.5 the stagnation region has a very small extension and the Nu/Nu_o contour map pattern is more similar to the one at R=2 rather than to the case R=1.

In order to understand the influence of the Reynolds number on the heat transfer, normalised Nusselt number maps at Re=2000 and Re=4000 are compared with the measurements at the higher Reynolds number shown in Fig. 8. Only the case R=3 is reported in Fig. 9, since the Reynolds number influence is quite similar for most of the blowing rates. For Re=2000 (see Fig. 9b) a slight asymmetry is visualized because, at such a low velocity, natural convection has a small contribution which cannot be neglected.

For increasing Re high heat transfer

regions on the upstream and downstream side of the jet become slightly larger while the normalised Nusselt number increase is quite evident from *Re*=2000 to 4000. At low Reynolds numbers, the iso-Nusselt maps are more elongated in the wake region, on the contrary, for high Reynolds numbers, the local maximum regions, which cover a smaller area and are located at about *x*/*D*=1, move upstream. This upwind shift may be attributed to a shift of both the CVP and the node in the jet downwind region (see Fig. 7) which are very energised.

4 Conclusions

In this paper convective heat transfer on a surface in the neighbourhood of a round jet in a crossflow and PIV measurements have been conducted. Tests have been performed at different Reynolds numbers and injection ratios, and the influence of these parameters is widely analysed. Flow field ant turbulence statistics measurements have been conducted in the symmetry plane of the jet and in the plane normal to the pipe axis located at a quarter of the pipe diameter from the wall. Results have shown that in the wake region convective heat transfer can be connected with the turbulent kinetic energy.

For *R*<1.5 a minimum in the heat transfer can be seen at about *x*/*D*=1, while two local maxima occur at *z*/*D*=±1 close to the pipe exit edges. This pattern is quite evident for *R*=0.5. The maxima tend to disappear for increasing velocity ratios, while, for *R*>1.5, the heat transfer minimum becomes a maximum which weakens and moves slightly downstream for further increase in the velocity ratios. Owing to the rising obstruction of the jet, the convective heat transfer over the wall decreases for increasing *R* on the jet upstream side.

The effect of the Reynolds number on heat transfer has also been analysed in the range of values going from 2000 to 8000 and for *R*=3. The main differences in the heat transfer maps, which result in an upward motion and a reduction of the maximum region for increasing Reynolds numbers, can be attributed to the change in the CVP shape and position.

References

[1] Eckert E R G. Analyses of film cooling and full coverage film cooling of gas turbine blades. ASME *J. Eng. Gas Turbine Power*, Vol. 106, No. 1, pp 206-213, 1984.

[2] Goldstein R J and Taylor J R. Mass transfer in the neighbourhood of jets entering a cross-flow. *J. Heat Transfer*, Vol. 104, pp 715-721, 1982.

[3] Leontiev A V. Heat and mass transfer problems for film cooling. ASME *J. Heat Transfer*, Vol. 121, pp 509-527, 1999.

[4] Gustafsson K M B and Johansson T G. An experimental study of surface temperature distribution on effusion-cooled plates. ASME *J. Eng. Gas Turbine Power*, Vol. 123, pp 308-316, 2001.

[5] Astarita T, Cardone G and Carlomagno G M. On the cooling of gas turbines. *J. flow visualization and image processing*, Vol. 8, pp 287-302, 2001.

[6] Foss J. Interaction region phenomena for the jet ina cross-flow problem. *Rep.* SFB 80/E7161*Univ. Karlsruhe*, 1980.

[7] Andreopoulos J and Rodi W. Experimental investigation of jets in a cross flow. *J. Fluid Mech.*, Vol. 138, pp 93-127, 1984.

[8] Fric T F and Roshko A. Vortical structures in the wake of a transverse jet. *J. Fluid Mech.*, Vol. 279, pp 1-47, 1994.

[9] Kelso R M, Lim T T and Perry A E. An experimental study of round jets in cross-flow. *J. Fluid Mech.*, Vol. 306, pp 111-144, 1996.

[10] Sykes R I, Lewellen W S and Parker S F. On the vorticity dynamics of a turbulent jet in a crossflow. *J. Fluid Mech.*, Vol. 168, pp 393-413, 1986.

[11] Coelho S R M and Hunt J C R. The dynamics of the near field of strong jets in cross-flow. *J. Fluid Mech.*, Vol. 200, pp 95-120, 1989.

[12] Yuan L L and Street R L. Trajectory and entrainment of a round jet in crossflow. *Physics of Fluids*, Vol. 10, pp 2323-2335, 1998.

[13] Yuan L L, Street R L and Ferziger J H. Large-eddy simulations of a round jet in crossflow. *J. Fluid Mech.*, Vol. 379, pp 71-104, 1999.

[14] Astarita T and Cardone G. Thermofluiddynamic analysis of the flow in a sharp 180° turn channel. *Exp. Thermal Fluid Sci.*, Vol. 20, pp 188-200, 2000.